Thermally conductive thin films derived from defect free graphene-natural rubber latex nanocomposite: Preparation and properties

CrossMark

Gejo George [a], Suja Bhargavan Sisupal [a], Teenu Tomy [a], Bincy Akkoli Pottammal [a], Alaganandam Kumaran [a], Vemparthan Suvekbala [a], Rajmohan Gopimohan [a], Swaminathan Sivaram [b], Lakshminarayanan Ragupathy [a, *]

[a] Corporate R&D Center, HLL Lifecare Limited, Akkulam, Sreekariyam (P.O.), Trivandrum, 695017, India
[b] Polymers and Advanced Materials Laboratory, National Chemical Laboratory, Dr. Homi Bhabha Road, Pune, 411008, India

ARTICLE INFO

ABSTRACT

Commercially useful rubber products *viz.* gloves, condoms, tyres, and rubber hoses used in high temperature environments, etc., require efficient thermal conductivity, which increases the lifetime of these products. Graphene can fetch this property, if it is effectively incorporated into the rubber matrix. The great challenge in preparing graphene-rubber nanocomposites is formulating a scalable method to produce defect free graphene and its homogeneous dispersion into polymer matrices through an aqueous medium. Here, we used a simple method to produce defect free few layer (2–5) graphene, which can be easily dispersed into natural rubber (NR) latex without adversely affecting its colloidal stability. The resulting new composite showed large increase in thermal conductivity (480–980%) along with 40% increase in tensile properties and 60% improvement in electrical conductivity. This study provides a novel and generalized approach for the preparation of graphene based thermally conductive rubber nanocomposites.

1. Introduction

Efficient heat dissipation in rubber based products is a desirable property, which will enhance the product durability and lifecycle. In the case of products such as gloves, condoms and footwear, effective heat dissipation could reduce the sweating and enhance the comfort levels as well as delay the product failure due to heat induced degradation of the rubber.

Conventionally, the target thermal conductivity values (>1 W/mK) can be achieved by dispersing high loadings (50–80 vol%) of the thermally conductive micron-size fillers in thermally insulating polymers (< 0.2 W/mK) [1]. However, such high filler loadings resulted in high density and expensive composites with poor mechanical properties all of which combined to limit their practical applications.

Graphene, a sp^2 hybridized two dimensional material, exhibits several unique properties such as (a) superior thermal conductivity (~5000 W/mK), (b) high modulus (~1100 GPa) (c) elasticity (20% of its initial length) and (d) high electrical conductivity (mobility of charge carriers 200,000 $cm^2 V^{-1} s^{-1}$) [2–5]. These properties have motivated the researchers to explore and develop new materials based on graphene for numerous applications ranging from advanced composites, semiconductor materials to biomedical devices [6,7].

In recent years, several methods have been reported for the preparation of defect free, monolayer to few and multiple layers graphene, graphene oxide (GO), reduced GO (rGO) as well as functionalized graphenes [8–11]. These diversities in graphene enable efficient modulation of interfacial adhesion and enhance its compatibility with number of polymers [12–19] such as polyaniline, polylactic acid, polycaprolactone, PEG etc. In general, graphene production methods can be categorized as two a) bottom-up methods (e.g. chemical vapour deposition and SiC) and b) top-down methods (e.g. high shear mixing, chemical exfoliation etc.) [20]. Bottom-up methods yield high quality of graphene with low number of defects and could be useful for electronic applications, however, they are expensive and difficult to produce in large scale [21]. On the contrary, top-down methods are scalable, less expensive and could be employed for the large scale applications such as conductive inks, fillers in composites, sensors and batteries. Thus,

* Corresponding author.
  E-mail addresses: laks@lifecarehll.com, laks77@gmail.com (L. Ragupathy).

several top-down methods *viz.* chemical exfoliation of graphite based on the Hummers method, solvent- and/or surfactant-assisted liquid-phase exfoliation, graphite intercalated compounds, electrochemical expansion and ball milling with triazine derivatives have been reported [11,22—26]. The later method could be employed to produce defect free few layers graphene that is suitable for preparing graphene-NR latex composites, because, it is easy to practice, environment friendly, inexpensive and the ingredients used do not adversely affect the NR latex colloidal stability. In this ball milling method, Leon et al. [11] tried five triazine derivatives as exfoliating agents to produce few layers graphene and found that 2,4,6-triamino-1,3,5-triazine (melamine) exhibited the best performance. However, it should be noted that this process may need modifications for taking the resulting graphene into the applications. No paper discusses an appropriate method to use this few layers graphene as a reinforcing material especially for NR latex.

Because of the remarkable properties of graphene and its diversities as well as possibilities for functionalization (both covalently and non-covalently), polymer-graphene nanocomposites have been extensively studied and reviewed [27—30]. However, only few studies are available on NR latex-graphene nanocomposites [31—37]. The general approach to fabricate graphene-NR Latex nanocomposites involves dispersing GO into NR latex, in-situ reduction using reducing agents (e.g. hydrazine hydrate), followed by coagulation, and compounding using a two roll mill [31—37]. However, this manner of preparation adversely impacts the colloidal stability of NR latex and cannot be used for producing dipped products. Moreover, the resulting composites showed only marginal increment in the thermal conductivity i.e. 13 and 40% of increment at 2 and 5 wt% rGO, respectively [33,35]. This may be because of the structural defects in rGO and its ability to aggregate during the in-situ reduction process. Furthermore, the unreduced oxygen functionalities in rGO may not interact well with the rubber matrix affecting a decrease in compatibility between the rubber and rGO. Recently, Iliut et al. [38] reported the fabrication of 0.08 wt % GO and ex-situ reduced GO incorporated NR latex nanocomposites. GO incorporated dip molded nanocomposite showed 3 MPa increase in tensile strength whereas rGO incorporated NR latex displayed a decrease in ultimate tensile strength.

In this paper, we report a simple and scalable method for producing defect free few (2—5) layers graphene dispersions and its NR latex nanocomposites for the first time. The obtained nanocomposites showed a significant improvement in thermal conductivity as well as substantial enhancement of mechanical properties and electrical conductivity.

2. Experimental

2.1. Materials

Graphite was purchased from Sigma Aldrich (No: 282863) and used without further purification. Melamine was procured from Sigma Aldrich (No: M2659). Distilled water was used for the preparation of graphene dispersions. Three different Carbon Blacks [high abrasion furnace (HAF 330), super abrasion furnace (SAF 220) and semi reinforcing filler (SRF)] were supplied by Philips Carbon Black Limited, India. Vulcanizing agent i.e. sulphur was purchased from Associates Chemicals, Kochi, India. Accelerator (dithio carbamates) and dispersing agents (Darvan-I and II) were procured from Vanderbilt, USA. Antioxidant (Wingstay − L) was purchased from Environ Chemicals, Mumbai. Casein was bought from Casein India, Mumbai, India. Double centrifuged natural rubber latex with 60% dry rubber content was obtained from St. Mary's Rubbers Pvt. Ltd., Kanjirappally, Kerala, India. The detailed procedure of latex compounding is provided in the supporting information.

2.2. Exfoliation of graphite using planetary ball milling and fabrication of graphene reinforced NR latex nanocomposites

Planetary ball milling was performed using a Fritsch Pulverisette 5 Classic Line with 4 grinding bowl fasteners using Yttria stabilized zirconia jars and zirconia grinding balls. In a typical experiment, the exfoliating agent melamine was ground with graphite (at a ratio of 3:1) at 100 rpm for 1 h (successive grinding for 1 h with 15 min grinding and 15 min pause). To provide a better stability for the aqueous dispersion, 12.5 wt% of Darvan-I, was also added during grinding. The ball milled material was then made as 30 wt% aqueous dispersion and probe sonicated (SONICS, 750 W for 2 min at 25% amplitude) to obtain defect free few layers graphene dispersion.

The graphene dispersion obtained as above was incorporated into compounded NR latex at different concentrations i.e. 0.3 [0.29], 0.7 [0.66], 1.5 [1.43], 3 [2.85] and 5 [4.75] parts per hundred gram of rubber (phr) [wt.%]. For proper mixing of graphene and NR latex, probe sonication was employed (750 W for 3 min at 20% amplitude). A lab model dipping machine was then used to fabricate the graphene reinforced NR latex nanocomposites thin films using two step dipping procedure and vulcanized in hot air oven at 80 °C for 45 min. The vulcanized samples were stripped out from the glass mold using silica powder. Then, they were kept at room temperature for 2—3 days for maturation and cut as ring samples (thickness: 40—60 μm) for tensile analysis.

For thermal conductivity measurements, 1.5 phr graphene-NR latex nanocomposite thin films along with control sample were cast on a glass plate surface with a final thickness of ~70 μm and with dimension 15 cm × 10 cm. The electrical conductivity measurements were performed on 1 mm thick sheets of control sample and 1.5 phr graphene-NR latex nanocomposite casted on the glass plate.

2.3. Characterization of graphene and graphene-NR latex nanocomposites

WAXS measurements were carried out on XEUSS SAXS/WAXS system using a Genix micro source from Xenocs operated at 50 kV and 0.6 mA. The Cu Kα radiation (1.54 Å) was collimated with FOX2D mirror and two pairs of scatter less slits from Xenocs. The 2D-patterns were recorded on a Mar345 image plate and processed using Fit2D software. All the measurements were made in the transmission mode.

Raman spectroscopy analysis was performed to both graphite and milled sample [graphite/melamine/darvan (G/M/D)] using Horiba Scientific LabRAM-HR Raman microscope. A 514 nm excitation laser and 1800 g/mm grating were used. Spectra were recorded with a 100× lens. Aqueous dispersion of G/M/D was drop casted on a glass plate and allowed to dry at 70 °C. Then, the glass plate (G/M/D) is carefully dipped in hot water (60—70 °C) for 5 times to remove the melamine and dried at 70 °C.

Transmission electron microscopy (TEM) was also used to investigate the produced graphenes. TEM specimen was prepared by drop casting the graphene dispersion onto a standard TEM grid. A JEOL JEM-2010 was used to analyze the samples at 200 kV. In the case of composite thin film samples, cryomicrotoming was employed to prepare the samples required for TEM analysis. The samples were first cooled to around −70 °C to reach below the T_g of natural rubber and microtomed and placed on the TEM grids.

Tensile testing of the ring samples was done on a Shimadzu AGX-10 universal testing machine (UTM) at a cross head speed of 500 mm/min and load cell 500 N according to ASTM D412 (circumference mean = 100 mm, width of the ring = 20 mm). The strain rate was calculated as 1666% min^{-1} [(cross head speed/gauge

length i.e. 30 mm) × 100]. For each set, 20—25 samples (thickness ~ 40—60 μm) were tested to obtain good uniform results with standard deviation.

Thermal conductivity of graphene-NR nanocomposites was measured using a HOT-DISK TPS 2500S Thermal Constants Analyzer. The thermal conductivity studies were performed in a muffle furnace, where the sample/sensor is put in a vertical set up and a weight with fixed mass (200/500 g) can be reproducibly placed on top of this stack. Each sample was allowed to reach a density in equilibrium with the applied load and the measurements were taken.

Electrical Conductivity of graphene-NR latex nanocomposites was measured using Hioki 3532-50 LCR Hitester using the two probe method. Round samples with 10 mm diameter, 1 mm thickness and coated with silver paste (silver in isoamyl acetate) to obtain good uniform contact with the electrodes were used. The analysis was performed in the frequency range 50 Hz to 5 MHz.

3. Results and discussion

3.1. Production of defect free few layers graphene by planetary ball milling

Shear induced chemical exfoliation of graphite to form few layer graphene appears to be a simple, scalable and low cost method. Accordingly graphite and melamine in 1:3 ratio was subjected to ball milling along with 12.5 wt% of Darvan-I (Sodium polynaphthalene sulphonate), an anionic surfactant, which helps to disperse the produced graphene in water. The ground mixture was then dispersed in water using a probe sonicator to obtain a stable dispersion, which was characterized by XRD, Raman spectroscopy and TEM. The dispersions were found to be stable at room temperature for as long as 6 weeks.

The XRD patterns of graphite and G/M/D dispersions (with a 1:3:0.125 wt ratio) before and after milling are shown in Fig. 1a. The sharp graphitic (002) reflection at around 27° clearly decreases after ball milling of graphite with melamine, indicating the exfoliation of graphite to graphene. The other small peaks at around 13, 15, 22, 27 and 30° are due to melamine. These observations are in good agreement with that of Leon et al. [11,26].

Raman spectroscopic analysis was also performed for G/M/D sample (Fig. 1b). Both graphite and graphene exhibit G and 2D peaks at 1580 and 2700 cm^{-1}, respectively. In addition, when graphene has defects, additional Raman peaks appear at 1345 cm^{-1} (D band) and 1626 cm^{-1} (D′ band). The latter appears as a shoulder on the G band and is characteristic of few layers graphene [11,39—43]. Graphite exhibits sharp and intense 2D band at 2700 cm^{-1}, whereas, for graphene the 2D band is shifted and appears as a broad peak. The deconvolution of 2D band results in four Lorentzian peaks, which are signatures of bi-layer graphene [11,41,42].

The nature of defects (e.g. sp^3, vacancy and edge) have also been determined using the intensity ratios between D and D′ bands ($I_D/I_{D'}$). $I_D/I_{D'}$ is ~13 for sp^3 type defects, decreases to ~7 for vacancy-like defects and reaches the minimum for boundary-like or edge like
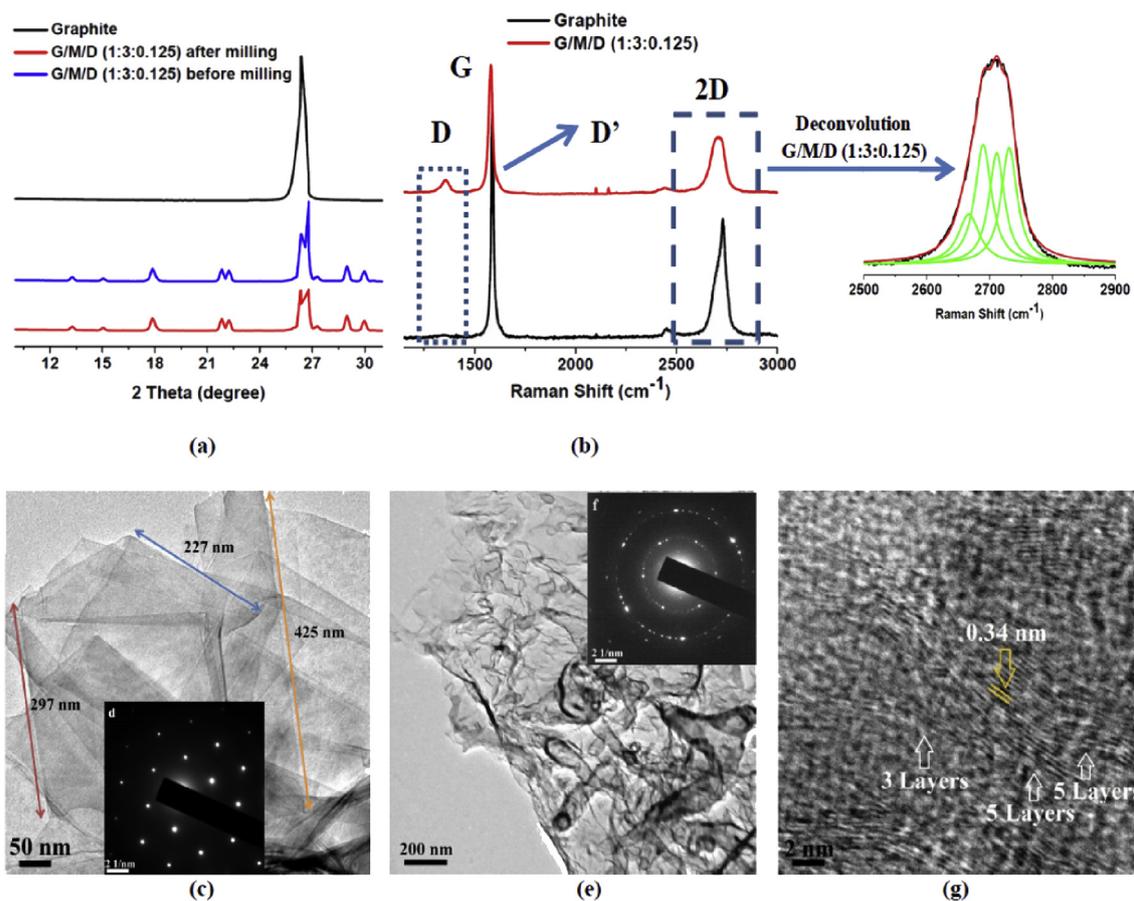
Fig. 1. Characterization of graphene samples produced using melamine as the exfoliating agent. (a) XRD, (b) Raman Spectra with deconvolution of 2D band, (c) TEM images of G/M/D dispersion in water showing sheet like structure, (d) SAED pattern of the graphene sheet, (e) TEM images of G/M/D dispersion in water showing large graphene flakes with wrinkles, (f) SAED pattern of the edge of the graphene flakes and (g) Graphene fringes observed in G/M/D sample with varying number of layers (3—5). (A colour version of this figure can be viewed online.)

defects [11,44,45]. The observed $I_D/I_{D'}$ values are much low ranging from 0.86 to 1.16 (Table S1), which indicates that the graphenes have only edge or boundary like defects and confirming that the milling process has not introduced any new vacancy or basal plane defects.

The TEM images clearly show the presence of both sheet like structures (Fig. 1c) as well as large flakes of graphene that form wrinkles (Fig. 1e), which may be due to their high flexibility [11,26]. In Fig. 1d, SAED pattern of the sheet like structure of graphene (Fig. 1c) shows one set of symmetric 6-fold diffraction spots. The outer group of diffraction spots is from equivalent planes (1–210), and is showing higher intensity than the inner set (1–100) and indicates a key factor for A–B stacking bilayer graphene [46–48]. In Fig. 1f, SAED pattern of the wrinkled flakes of graphene (given in Fig. 1e) show that most regions of the graphene film has a hexagonal diffraction pattern, indicating the crystalline nature of the film. The multiple sets of diffraction in this SAED pattern signpost the presence of few layer graphene [46–48]. In addition, the graphene fringes (Fig. 1g) corresponding to 3 and 5 layers graphene is also clearly visible. Based on the Raman and TEM analysis, we claim that the produced graphene in this study as few (2–5) layers defect free graphene. The lengths of the graphene sheets are observed to be ~220–450 nm.

We performed thermogravimetric analysis (TGA) to investigate the insights into the composition of graphite, exfoliating agent and surfactant after ball milling as well as how much the hot water washing helps to purify the sample. Thus, ball milled sample (G/M/D), graphite, melamine, Darvan-I and purified ball milled sample using hot water (70 °C) were analyzed by TGA (Fig. S3). Graphite is thermally stable when heated up to 900 °C under inert atmosphere. Weight loss at 350 °C (73%) corresponds to the amount of melamine used for ball milling. The amount of Darvan-I used is only 3%, a corresponding weight loss at 500 °C in the milled sample is also observed. Ball milled sample (G/M/D) show 24% of graphene, which is equal to the amount of graphite employed in this study. There is no additional loss taking place above or below this temperature, showing that no oxidative defects have been produced around the graphite flakes during grinding [11,26]. Furthermore, TGA indicates that the hot water washing removes the melamine and produces graphene with purity of ~95%.

3.2. Incorporation of graphene into NR latex and fabrication of graphene-NR latex nanocomposite

Incorporation of graphene into NR latex without affecting its colloidal stability is a significant challenge especially under high shear. We used a probe sonication method for the preparation of stable aqueous dispersions of graphene as well as to incorporate the graphene dispersion into compounded NR latex. This method provides a stable graphene incorporated NR latex and could be used for the fabrication of both dip molded and dry rubber products.

To investigate the effect of graphene content on the NR latex, different concentrations of graphene [0.3 (0.29), 0.7 (0.66), 1.5 (1.43), 3 (2.85) and 5 (4.75) phr (wt.%)] were incorporated into the NR latex and nanocomposite thin films were produced (Fig. 2). Four control samples based on NR latex were also made; (a) only compounded NR latex (no graphene), (b) melamine (milled melamine/Darvan-I), (c) graphite (only milled graphite) and (d) three different carbon blacks (high abrasion furnace/semi-reinforced/super abrasion furnace).

Tensile properties of composite samples thus obtained i.e. tensile strength (TS), tensile modulus (TM) and elongation at break (EB) were determined and given in Fig. 3b and Table 1. Representative stress-strain curves of the control and composite samples are shown in Fig. 3a. Compared to the control sample (a), a 0.3 phr graphene incorporated composite shows 15% increment in TS (6% increase of TM) while 0.7 phr graphene displays 37% rise in TS (6% increase of TM). Further increasing the graphene content to 1.5 phr results in a 40% increment of TS (25% increase of TM). At 0.3 and 0.7 phr graphene loading, the increment of TM is observed to be minimum (6%) compared to control NR sample. At the same time, compared to melamine control, there is no change in TM. This suggests that >0.7 phr graphene may be required to reduce the onset of strain induced crystallization [49], which could possibly increase the tensile modulus. Interestingly, EB for the samples produced (from 0.3 to 1.5 phr graphene) is 800–850%, which is similar to the control sample (a). On further increasing the graphene content i.e. 3 and 5 phr graphene, results in decrease of tensile properties (Table 1) possibly a consequence of graphene agglomeration. Tensile properties of other control samples (b), (c), and (d) are similar to the tensile properties of the control sample

Fig. 2. Production process of graphene reinforced NR latex nanocomposites (a) Sonication followed by (b) first dipping of the mould, (c) second dipping and finally (d) vulcanization in hot air oven. The produced NR latex control sample (e) was kept on a printed paper along with graphene-NR latex nanocomposites thin films (1.5 phr) (f) to test the transparency of both samples. (A colour version of this figure can be viewed online.)
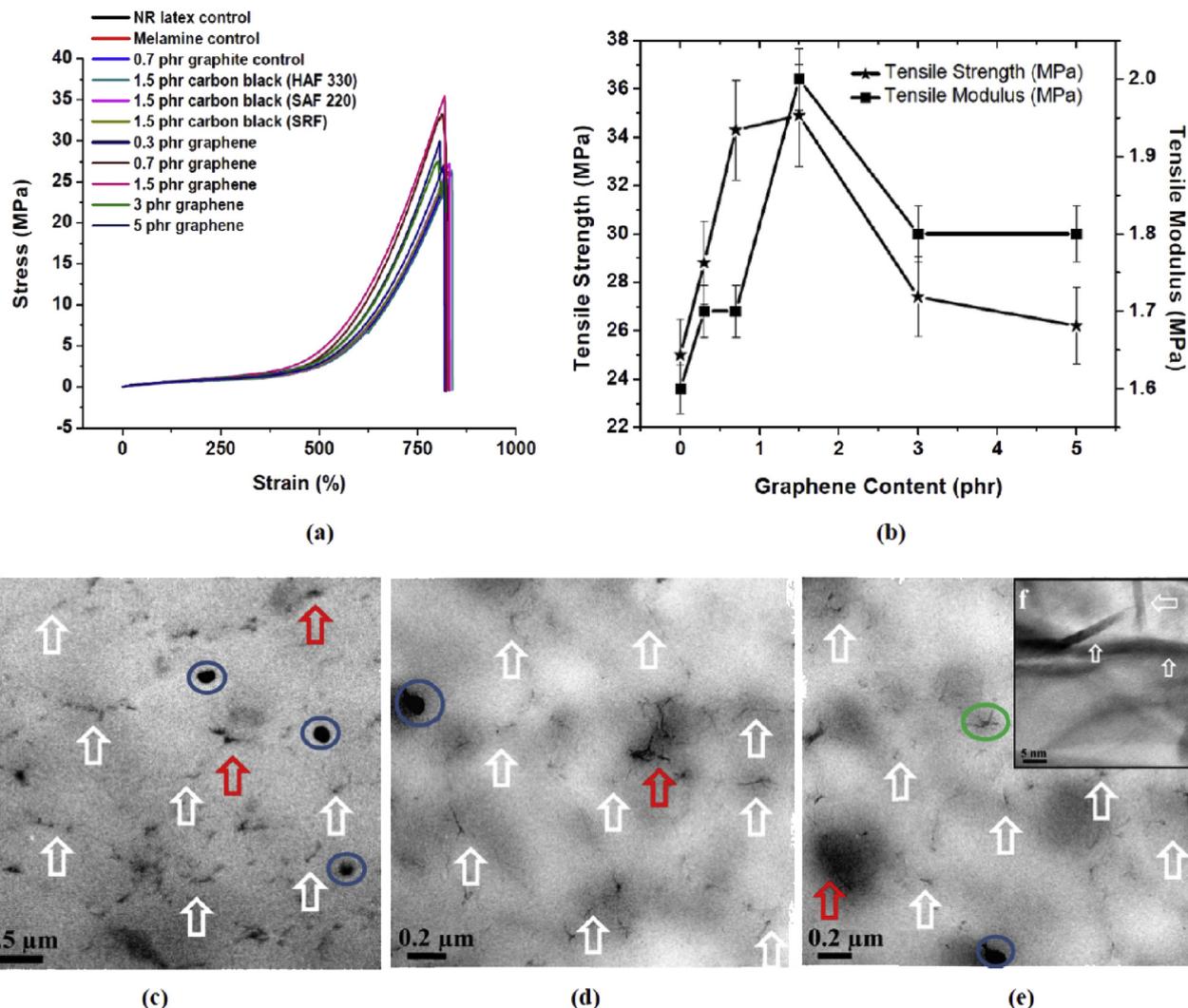
Fig. 3. (a) Representative stress-strain curves of all the control samples and graphene-NR latex nanocomposite samples, b) Tensile properties of graphene reinforced NR latex composites, (c), (d) and (e) TEM images of graphene-NR latex nanocomposite thin films (1.5 phr), (f) HRTEM image of 1.5 phr graphene-NR latex nanocomposite thin film (area marked as green circle in Fig. 3e). (A colour version of this figure can be viewed online.)

(a). This confirms the beneficial effect of graphene on the improvement in the tensile properties of graphene-NR latex composites.

When a graphene-NR latex nanocomposite is prepared using GO followed by chemical reduction route, significantly larger increase in tensile modulus compared to tensile strength is observed [31–37,50]. The oxygen functionalities in rGO (C−O, C=O and

O−C=O) have a strong influence on the NR-latex vulcanization kinetics and increases the crosslinking density [36,51]. This may not be happening in the present study as we are using the defect free few layer graphene for the composite fabrication. Therefore, a noteworthy increase in tensile strength and modest increment in modulus without any adverse impact on elongation are observed. These properties could be useful to make the products for skin

Table 1
Tensile properties of graphene reinforced NR latex nanocomposites along with the control samples.

Category	Sample	Tensile strength (MPa)	Tensile Modulus (MPa)	Elongation at break (%)
Controls	NR Latex	25.0 ± 1.5	1.6 ± 0.03	869
	Melamine Control	25.8 ± 2.0	1.7 ± 0.02	865
	Control (0.7 phr Graphite)	25.9 ± 2.0	1.5 ± 0.02	856
	1.5 phr Carbon black (HAF 330)	26.1 ± 1.6	1.4 ± 0.02	861
	1.5 phr Carbon black (SAF 220)	27.4 ± 1.7	1.5 ± 0.02	860
	1.5 phr Carbon black (SRF)	25.2 ± 1.5	1.4 ± 0.02	854
G/M/D	0.3 phr Graphene	28.8 ± 1.7	1.7 ± 0.03	807
	0.7 phr Graphene	34.3 ± 2.0	1.7 ± 0.03	834
	1.5 phr Graphene	34.9 ± 2.0	2.0 ± 0.04	820
	3 phr Graphene	27.4 ± 1.6	1.8 ± 0.03	850
	5 phr Graphene	26.2 ± 1.5	1.8 ± 0.03	851

contact applications.

A thin film made from NR-latex is transparent, which is a desirable property to make condoms, gloves, balloons etc. Transparency of polymer composites depends on the size and volume of the reinforcing particles (causes structural and compositional heterogeneities) as well as its homogeneous distribution into polymer matrix [52]. Graphene is a 2-dimensional material and has huge surface area, when it is incorporated into NR latex, it provides an opportunity to increase the mechanical, thermal and electrical properties at lower volumes without compromising the auxiliary characteristics such as optical transparency. Therefore, the produced 1.5 phr graphene incorporated thin films of the composites are observed to be transparent (Fig. 2f) and nearly similar to the control NR latex sample (Fig. 2e). By increasing the amount of graphene to 3 and 5 phr, the transparency is observed to be reduced (Fig. S7). In contrary, transparency of 1.5 phr carbon black incorporated NR latex thin film (Fig. S7) is observed as very low, which could be due to the combination effects of higher particle size, aggregation and inhomogeneous distribution of the carbon black.

The TEM images of 1.5 phr graphene-NR latex nanocomposite films are shown in Fig. 3c–e. The images exhibit network like graphene structures. The incorporated graphene appears predominantly in an exfoliated form. TEM images clearly show that few layers of graphene (marked as white arrows) are evenly and uniformly distributed into the NR latex matrix. Stacked graphene (~>10 layers) is also observed and marked as red arrows. The blue circles correspond to agglomerated graphene, which is seen even at 1.5 phr graphene incorporated NR latex. However, above 1.5 phr graphene content, the degree of agglomeration is detected as very high. This may be due to the strong forces of attraction between individual graphene layers/sheets [50]. The HR-TEM image (Fig. 3f) of the green circled portion in Fig. 3e reveals the presence of exfoliated graphene in NR latex matrix with thickness ranging from 2 to 3 nm.

3.3. Thermal conductivity of graphene-NR nanocomposite thin films

Following samples were used for thermal conductivity studies using TPS 2500 S Hot Disk Thermal Constants Analyzer; film made from (i) NR latex and (ii) 1.5 phr (1.43 wt%) G/M/D incorporated NR latex (G/M/D-NR). Experiments were performed at two different temperatures i.e. 23 and 37 °C (Table 2). During the analysis, 200 g weight was applied at 23 °C whereas two different weights (200 and 500 g) were exerted at 37 °C. For the applications like gloves, condoms, footwear etc., require human contact where the different forces are applied during usage. Hence, at 37 °C, 200 and 500 g weights were applied to investigate the influence of different weights on thermal conductivity. Compared to the NR latex control sample (0.065 W/mK), G/M/D-NR (0.379 W/mK) shows 480% increment at 23 °C. At 37 °C, G/M/D-NR displays 490% (Control: 0.073 W/mK and G/M/D-NR: 0.428 W/mK) and 980% (Control: 0.084 W/mK and G/M/D-NR: 0.910 W/mK) increment with 200 and 500 g weights, respectively. The values reported herein, a

500–1000% increase in thermal conductivity is far superior to what has been previously reported with graphene-NR nanocomposites prepared using rGO [33,35]. Achieving higher thermal conductivity in graphene-polymer nanocomposites is often limited by mainly two parameters: (i) quality of graphene (isotopes, defects, impurities or vacancies) and (2) the large interfacial thermal resistance between the polymer mediated graphene boundaries. Consequently, previous studies employed high loading of graphene (up to 25 wt%) into polymer matrix to achieve a considerable increase in thermal conductivity [53]. In the present work, substantial improvements in thermal conductivity of the composites have been achieved without loss of physical properties of the components.

3.4. Electrical conductivity of graphene-NR nanocomposite

To evaluate the electrical conductivity of graphene reinforced [1.5 phr (1.43 wt%)] NR latex nanocomposite sample, two probe method was employed since it is frequently employed for NR latex based composites [33,54]. Graphene reinforced NR latex nanocomposite (1.5 phr) shows 60% increment in electrical conductivity (S/m) at 5 MHz frequency compared to that of the control sample (Control = 4.56×10^{-4} S/m and 1.5 phr GMD = 7.31×10^{-4} S/m) (Fig. 4). Earlier studies have reported good thermal and electrical properties for graphene reinforced composites owing to well organized microstructures [55]. The reported electrical conductivity of rGO-NR latex nanocomposites varies from 66% (at 3 wt%) to ~ 5 orders of magnitude increment, which largely depends on how the rGO forms interconnected networks within the rubber matrix [35,56,57] and the processing conditions. This is the first report of electrical conductivity of defect free few layers graphene-NR latex nanocomposite.

4. Conclusions

A simple and scalable method to produce defect free few layers graphene that is highly suitable to prepare graphene-NR latex nanocomposites is demonstrated. Using probe sonication, the graphene-aqueous dispersion was successfully incorporated into NR latex without affecting its colloidal stability. The graphene-NR latex nanocomposite showed enhanced thermal conductivity (480–980%) along with 40% increase in tensile strength and 60% rise in electrical conductivity. To the best of our knowledge such a

Table 2
Thermal conductivity values of graphene reinforced NR latex nanocomposites.

	Thermal Conductivity in W/mK at 23 °C	Thermal Conductivity in W/mK at 37 °C	
	200 g	200 g	500 g
NR latex thin film	0.065	0.073	0.084
1.5 phr G/M/D incorporated NR latex thin film	0.379	0.428	0.910
% increment	483	486	983
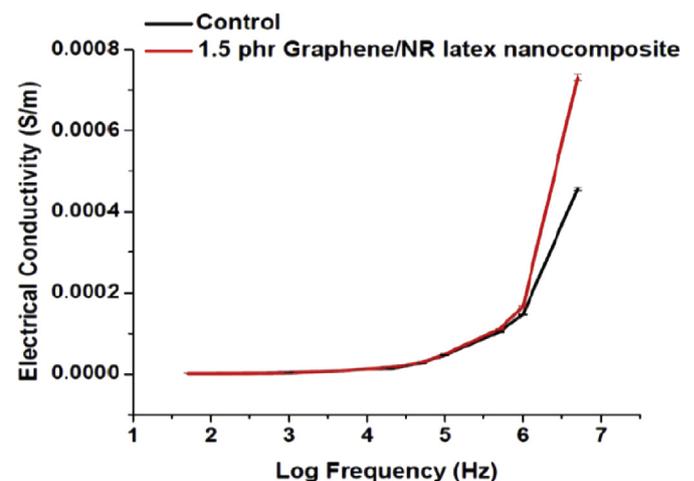
Fig. 4. Effect of graphene content on the conductivity of graphene reinforced NR latex nanocomposites as a function of log frequency. (A colour version of this figure can be viewed online.)

combination of properties in graphene-NR nanocomposites is unprecedented in the literature. Our studies established comprehensively the "proof of principle" that well dispersed and stable aqueous dispersions of few layer graphene-NR latex nanocomposites is a desirable precursor for producing new generation of rubber-graphene composites for numerous applications. Furthermore, this concept can be adopted to produce a range of defect free few layer graphene-synthetic latexes/emulsions/polymer dispersions based nanocomposites to significantly enhance its physical, mechanical, thermal and electrical properties.

Acknowledgements

Appendix A. Supplementary data

Supplementary data related to this article can be found at http://dx.doi.org/10.1016/j.carbon.2017.04.068.

References

[1] M. Shtein, R. Nadiv, M. Buzaglo, K. Kahil, O. Regev, Thermally conductive graphene-polymer composites: size, percolation, and synergy effects, Chem. Mater 27 (2015) 2100–2106, http://dx.doi.org/10.1021/cm504550e.

[2] A.K. Geim, K.S. Novoselov, The rise of graphene, Nat. Mater 6 (2007) 183–191, http://dx.doi.org/10.1038/nmat1849.

[3] K.S. Novoselov, V.I. Fal'ko, L. Colombo, P.R. Gellert, M.G. Schwab, K. Kim, A roadmap for graphene, Nature 490 (2012) 192–200, http://dx.doi.org/10.1038/nature11458.

[4] A.A. Balandin, S. Ghosh, W. Bao, I. Calizo, D. Teweldebrhan, F. Miao, C.N. Lau, Superior thermal conductivity of single-layer graphene, Nano Lett. 8 (2008) 902–907, http://dx.doi.org/10.1021/nl0731872.

[5] R.R. Nair, P. Blake, A.N. Grigorenko, K.S. Novoselov, T.J. Booth, T. Stauber, et al., Fine structure constant defines visual transparency of graphene, Science 320 (2008) 1308, http://dx.doi.org/10.1126/science.1156965.

[6] X. Huang, X. Qi, F. Boey, H. Zhang, Graphene-based composites, Chem. Soc. Rev. 41 (2012) 666–686, http://dx.doi.org/10.1039/C1CS15078B.

[7] X. Ji, Y. Xu, W. Zhang, L. Cui, J. Liu, Review of functionalization, structure and properties of graphene/polymer composite fibers, Compos. Part A Appl. Sci. Manuf. 87 (2016) 29–45, http://dx.doi.org/10.1016/j.compositesa.2016.04.011.

[8] J.Y. Baek, I.-Y. Jeon, J.-B. Baek, ge-iodine/sulfonic acid-functionalized graphene nanoplatelets as efficient electrocatalysts for oxygen reduction reaction, J. Mater. Chem. A 2 (2014) 8690–8695, http://dx.doi.org/10.1039/C4TA00927D.

[9] I.-Y. Jeon, H.-J. Choi, S.-M. Jung, J.-M. Seo, M.-J. Kim, L. Dai, et al., Large-scale production of edge-selectively functionalized graphene nanoplatelets via ball milling and their use as metal-free electrocatalysts for oxygen reduction reaction, J. Am. Chem. Soc. 135 (2013) 1386–1393, http://dx.doi.org/10.1021/ja3091643.

[10] R.S. Edwards, K.S. Coleman, Graphene synthesis: relationship to applications, Nanoscale 5 (2013) 38–51, http://dx.doi.org/10.1039/C2NR32629A.

[11] V. León, A.M. Rodriguez, P. Prieto, M. Prato, E. Vázquez, Exfoliation of graphite with triazine derivatives under ball-milling conditions: preparation of few-layer graphene via selective noncovalent interactions, ACS Nano 8 (2014) 563–571, http://dx.doi.org/10.1021/nn405148t.

[12] R. Jain, A. Sinha, N. Kumari, A.L. Khan, A polyaniline/graphene oxide nanocomposite as a voltammetric sensor for electroanalytical detection of clonazepam, Anal. Methods 8 (2016) 3034–3045, http://dx.doi.org/10.1039/C6AY00424E.

[13] D. Gui, C. Liu, F. Chen, J. Liu, Preparation of polyaniline/graphene oxide nanocomposite for the application of supercapacitor, Appl. Surf. Sci. 307 (2014) 172–177, http://dx.doi.org/10.1016/j.apsusc.2014.04.007.

[14] C. Hu, Z. Li, Y. Wang, J. Gao, K. Dai, G. Zheng, et al., Comparative assessment of the strain-sensing behaviors of polylactic acid nanocomposites: reduced graphene oxide or carbon nanotubes, J. Mater. Chem. C 5 (2017) 2318–2328, http://dx.doi.org/10.1039/C6TC05261D.

[15] Q. Chen, J.D. Mangadlao, J. Wallat, A. De Leon, J.K. Pokorski, R.C. Advincula, 3D printing biocompatible polyurethane/poly(lactic acid)/graphene oxide nanocomposites: anisotropic properties, ACS Appl. Mater. Interfaces 9 (2017) 4015–4023, http://dx.doi.org/10.1021/acsami.6b11793.

[16] J. Song, H. Gao, G. Zhu, X. Cao, X. Shi, Y. Wang, The preparation and characterization of polycaprolactone/graphene oxide biocomposite nanofiber

[17] S. Ramazani, M. Karimi, Aligned poly(ε-caprolactone)/graphene oxide and reduced graphene oxide nanocomposite nanofibers: morphological, mechanical and structural properties, Mater. Sci. Eng. C 56 (2015) 325–334, http://dx.doi.org/10.1016/j.msec.2015.06.045.

[18] K. Yang, L. Feng, H. Hong, W. Cai, Z. Liu, Preparation and functionalization of graphene nanocomposites for biomedical applications, Nat. Protoc. 8 (2013) 2392–2403, http://dx.doi.org/10.1038/nprot.2013.146.

[19] A.M. Díez-Pascual, A.L. Díez-Vicente, Poly(propylene fumarate)/polyethylene glycol-modified graphene oxide nanocomposites for tissue engineering, ACS Appl. Mater. Interfaces 8 (2016) 17902–17914, http://dx.doi.org/10.1021/acsami.6b05635.

[20] M. Yi, Z. Shen, A review on mechanical exfoliation for the scalable production of graphene, J. Mater. Chem. A 3 (2015) 11700–11715, http://dx.doi.org/10.1039/C5TA00252D.

[21] D. Wei, B. Wu, Y. Guo, G. Yu, Y. Liu, Controllable chemical vapor deposition growth of few layer graphene for electronic devices, Acc. Chem. Res. 46 (2013) 106–115, http://dx.doi.org/10.1021/ar300103f.

[22] J. Wang, K.K. Manga, Q. Bao, K.P. Loh, High-yield synthesis of few-layer graphene flakes through electrochemical expansion of graphite in propylene carbonate electrolyte, J. Am. Chem. Soc. 133 (2011) 8888–8891, http://dx.doi.org/10.1021/ja203725d.

[23] K. Parvez, Z.-S. Wu, R. Li, X. Liu, R. Graf, X. Feng, et al., Exfoliation of graphite into graphene in aqueous solutions of inorganic salts, J. Am. Chem. Soc. 136 (2014) 6083–6091, http://dx.doi.org/10.1021/ja5017156.

[24] Y. Hernandez, V. Nicolosi, M. Lotya, F.M. Blighe, Z. Sun, S. De, et al., High-yield production of graphene by liquid-phase exfoliation of graphite, Nat. Nano 3 (2008) 563–568, http://dx.doi.org/10.1038/nnano.2008.215.

[25] C.-J. Shih, A. Vijayaraghavan, R. Krishnan, R. Sharma, J.-H. Han, M.-H. Ham, et al., Bi- and trilayer graphene solutions, Nat. Nano 6 (2011) 439–445, http://dx.doi.org/10.1038/nnano.2011.94.

[26] V. Leon, M. Quintana, M.A. Herrero, J.L.G. Fierro, A. de la Hoz, M. Prato, et al., Few-layer graphenes from ball-milling of graphite with melamine, Chem. Commun. 47 (2011) 10936–10938, http://dx.doi.org/10.1039/C1CC14595A.

[27] P. Dubey, P. Gopinath, PEGylated graphene oxide based nanocomposite grafted chitosan/polyvinyl alcohol nanofiber as an advanced antibacterial wound dressing, RSC Adv. (2016), http://dx.doi.org/10.1039/C6RA12192F.

[28] Y. Qin, Q. Peng, Y. Ding, Z. Lin, C. Wang, Y. Li, et al., Lightweight, superelastic, and mechanically flexible graphene/polyimide nanocomposite foam for strain sensor application, ACS Nano 9 (2015) 8933–8941, http://dx.doi.org/10.1021/acsnano.5b02781.

[29] S. Cho, M. Kim, J.S. Lee, J. Jang, Polypropylene/polyaniline nanofiber/reduced graphene oxide nanocomposite with enhanced electrical, dielectric, and ferroelectric properties for a high energy density capacitor, ACS Appl. Mater. Interfaces 7 (2015) 22301–22314, http://dx.doi.org/10.1021/acsami.5b05467.

[30] N.J. Kaleekkal, A. Thanigaivelan, M. Durga, R. Girish, D. Rana, P. Soundararajan, et al., Graphene oxide nanocomposite incorporated poly(ether imide) mixed matrix membranes for in vitro evaluation of its efficacy in blood purification applications, Ind. Eng. Chem. Res. 54 (2015) 7899–7913, http://dx.doi.org/10.1021/acs.iecr.5b01655.

[31] D.G. Papageorgiou, I.A. Kinloch, R.J. Young, Graphene/elastomer nanocomposites, Carbon N. Y. 95 (2015) 460–484, http://dx.doi.org/10.1016/j.carbon.2015.08.055.

[32] B. Dong, C. Liu, L. Zhang, Y. Wu, Preparation, fracture, and fatigue of exfoliated graphene oxide/natural rubber composites, RSC Adv. 5 (2015) 17140–17148, http://dx.doi.org/10.1039/C4RA17051B.

[33] J.R. Potts, O. Shankar, L. Du, R.S. Ruoff, Processing–morphology–property relationships and composite theory analysis of reduced graphene oxide/natural rubber nanocomposites, Macromolecules 45 (2012) 6045–6055, http://dx.doi.org/10.1021/ma300706k.

[34] H. Yang, P. Liu, T. Zhang, Y. Duan, J. Zhang, Fabrication of natural rubber nanocomposites with high graphene contents via vacuum-assisted self-assembly, RSC Adv. 4 (2014) 27687–27690, http://dx.doi.org/10.1039/C4RA02950J.

[35] Y. Zhan, J. Wu, H. Xia, N. Yan, G. Fei, G. Yuan, Dispersion and exfoliation of graphene in rubber by an ultrasonically-assisted latex mixing and in situ reduction process, Macromol. Mater. Eng. 296 (2011) 590–602, http://dx.doi.org/10.1002/mame.201000358.

[36] N. Yan, G. Buonocore, M. Lavorgna, S. Kaciulis, S.K. Balijepalli, Y. Zhan, H. Xia, L. Ambrosio, The role of reduced graphene oxide on chemical, mechanical and barrier properties of natural rubber composites, Compos. Sci. Technol. 102 (2014) 74–81, http://dx.doi.org/10.1016/j.compscitech.2014.07.021.

[37] D.C. Stanier, A.J. Patil, C. Sriwong, S.S. Rahatekar, J. Ciambella, The reinforcement effect of exfoliated graphene oxide nanoplatelets on the mechanical and viscoelastic properties of natural rubber, Compos. Sci. Technol. 95 (2014) 59–66, http://dx.doi.org/10.1016/j.compscitech.2014.02.007.

[38] M. Iliut, C. Silva, S. Herrick, M. McGlothlin, A. Vijayaraghavan, Graphene and water-based elastomers thin-film composites by dip-moulding, Carbon N. Y. 106 (2016) 228–232, http://dx.doi.org/10.1016/j.carbon.2016.05.032.

[39] A.C. Ferrari, J.C. Meyer, V. Scardaci, C. Casiraghi, M. Lazzeri, F. Mauri, et al., Raman spectrum of graphene and graphene layers, Phys. Rev. Lett. 97 (2006) 187401, http://dx.doi.org/10.1103/PhysRevLett.97.187401.

[40] D. Yoon, H. Moon, H. Cheong, J. Choi, J. Choi, B. Park, Variations in the raman spectrum as a function of the number of graphene layers, J. Korean Phys. Soc.

55 (2009) 1299—1303, http://dx.doi.org/10.3938/jkps.55.1299.

[41] A.C. Ferrari, D.M. Basko, Raman spectroscopy as a versatile tool for studying the properties of graphene, Nat. Nano 8 (2013) 235—246, http://dx.doi.org/10.1038/nnano.2013.46.

[42] A. Reina, J. Kong, M.S. Dresselhaus, Geometrical approach for the study of {G} band in the Raman spectrum of monolayer graphene, bilayer graphene, and bulk graphite, Phys. Rev. B 77 (2008) 245408, http://dx.doi.org/10.1103/PhysRevB.77.245408.

[43] W. Zhao, M. Fang, F. Wu, H. Wu, L. Wang, G. Chen, Preparation of graphene by exfoliation of graphite using wet ball milling, J. Mater. Chem. 20 (2010) 5817—5819, http://dx.doi.org/10.1039/C0JM01354D.

[44] A. Eckmann, A. Felten, A. Mishchenko, L. Britnell, R. Krupke, K.S. Novoselov, et al., Probing the nature of defects in graphene by raman spectroscopy, Nano Lett. 12 (2012) 3925—3930, http://dx.doi.org/10.1021/nl300901a.

[45] K.R. Paton, E. Varrla, C. Backes, R.J. Smith, U. Khan, A. O'Neill, et al., Scalable production of large quantities of defect-free few-layer graphene by shear exfoliation in liquids, Nat. Mater 13 (2014) 624—630, http://dx.doi.org/10.1038/nmat3944.

[46] Y. Zhang, L. Zhang, P. Kim, M. Ge, Z. Li, C. Zhou, Vapor trapping growth of single-crystalline graphene flowers: synthesis, morphology, and electronic properties, Nano Lett. 12 (2012) 2810—2816, http://dx.doi.org/10.1021/nl300039a.

[47] K. Yan, H. Peng, Y. Zhou, H. Li, Z. Liu, Formation of bilayer bernal graphene: layer-by-layer epitaxy via chemical vapor deposition, Nano Lett. 11 (2011) 1106—1110, http://dx.doi.org/10.1021/nl104000b.

[48] L.-H. Liu, J. Lyu, T.-K. Zhao, T.-H. Li, Large area preparation of multilayered graphene films by chemical vapour deposition with high electrocatalytic activity toward hydrogen peroxide, Mater. Technol. 30 (2015) 121—126, http://dx.doi.org/10.1080/10667857.2015.1112584.

[49] B. Ozbas, S. Toki, B.S. Hsiao, B. Chu, R.A. Register, I.A. Aksay, et al., Strain-induced crystallization and mechanical properties of functionalized graphene sheet-filled natural rubber, J. Polym. Sci. Part B Polym. Phys. 50 (2012) 718—723, http://dx.doi.org/10.1002/polb.23060.

[50] S. Yaragalla, A.P. Meera, N. Kalarikkal, S. Thomas, Chemistry associated with natural rubber—graphene nanocomposites and its effect on physical and structural properties, Ind. Crops Prod. 74 (2015) 792—802, http://dx.doi.org/10.1016/j.indcrop.2015.05.079.

[51] J. Wu, W. Xing, G. Huang, H. Li, M. Tang, S. Wu, Y. Liu, Vulcanization kinetics of graphene/natural rubber nanocomposites, Polym. Guildf. 54 (2013) 3314—3323, http://dx.doi.org/10.1016/j.polymer.2013.04.044.

[52] S. Ehlert, C. Stegelmeier, D. Pirner, S. Förster, A general route to optically transparent highly filled polymer nanocomposites, Macromolecules 48 (2015) 5323—5327, http://dx.doi.org/10.1021/acs.macromol.5b00565.

[53] W. Guo, G. Chen, Fabrication of graphene/epoxy resin composites with much enhanced thermal conductivity via ball milling technique, J. Appl. Polym. Sci. 131 (2014), http://dx.doi.org/10.1002/app.40565 n/a-n/a.

[54] M. Hernández, M. del M. Bernal, R. Verdejo, T.A. Ezquerra, M.A. López-Manchado, Overall performance of natural rubber/graphene nanocomposites, Compos. Sci. Technol. 73 (2012) 40—46, http://dx.doi.org/10.1016/j.compscitech.2012.08.012.

[55] Y. Luo, P. Zhao, Q. Yang, D. He, L. Kong, Z. Peng, Fabrication of conductive elastic nanocomposites via framing intact interconnected graphene networks, Compos. Sci. Technol. 100 (2014) 143—151, http://dx.doi.org/10.1016/j.compscitech.2014.05.037.

[56] Y. Zhan, M. Lavorgna, G. Buonocore, H. Xia, Enhancing electrical conductivity of rubber composites by constructing interconnected network of self-assembled graphene with latex mixing, J. Mater. Chem. 22 (2012) 10464, http://dx.doi.org/10.1039/c2jm31293j.

[57] C.H. Chan, Y.S. Ri Hanum, Y. Srinivasarao, K. Nandakumar, T. Sabu, Electrical properties of graphene filled natural rubber composites, Prog. Polym. Rubber Technol. Trans. Tech. Publ. (2013) 263—266, http://dx.doi.org/10.4028/www.scientific.net/AMR.812.263.